

Magnetic moment of rare earth elements in $R_2\text{Fe}_{14}\text{B}$ estimated with $\mu^+\text{SR}$

Jun Sugiyama^{1,*}, Kazutoshi Miwa¹, Hiroshi Nozaki¹, Yuji Kaneko¹, Bassam Hitti²,
Donald Arseneau², Gerald D Morris², Eduardo J. Ansaldo³, and Jess H. Brewer^{2,4}

¹*Toyota Central Research & Development Laboratories Inc., Nagakute, Aichi 480-1192, Japan*

²*TRIUMF, 4004 Wesbrook Mall, Vancouver, BC, V6T 2A3 Canada*

³*Department of Physics & Engineering Physics, University of Saskatchewan, Saskatoon, SK, S7N 5E2 Canada and*

⁴*Department of Physics & Astronomy, University of British Columbia, Vancouver, BC, V6T 1Z1 Canada*

(Dated: May 2, 2019)

The ferromagnetic (FM) nature of $\text{Nd}_2\text{Fe}_{14}\text{B}$ has been investigated with muon spin rotation and relaxation ($\mu^+\text{SR}$) measurements on an aligned, sintered plate-shaped sample. A clear muon spin precession frequency (f_{FM}) corresponding to the static internal FM field at the muon site showed an order parameter-like temperature dependence and disappeared above around 582 K ($\sim T_C$). This indicated that the implanted muons are static in the $\text{Nd}_2\text{Fe}_{14}\text{B}$ lattice even at temperatures above around 600 K. Using the predicted muon site and local spin densities predicted by DFT calculations, the ordered Nd moment (M_{Nd}) was estimated to be $3.31 \mu_B$ at 5 K, when both M_{Fe} and M_{Nd} are parallel to the \hat{c} -axis and $M_{\text{Fe}} = 2.1 \mu_B$. Furthermore, M_R in $R_2\text{Fe}_{14}\text{B}$ with $R = \text{Y}, \text{Ce}, \text{Pr}, \text{Sm}, \text{Gd}, \text{Tb}, \text{Dy}, \text{Ho}, \text{Er},$ and Tm was estimated from f_μ values reported in earlier $\mu^+\text{SR}$ work, using the FM structure proposed by neutron scattering and the same muon site and local spin density as in $\text{Nd}_2\text{Fe}_{14}\text{B}$. Such estimations yielded M_R values consistent with those obtained by the other methods.

PACS numbers: 76.75.+i, 75.50.Ee, 71.15.Mb

I. INTRODUCTION

Among many permanent magnet materials, $\text{Nd}_2\text{Fe}_{14}\text{B}$ ¹ and related intermetallic compounds² are known to be very suitable for industrial applications, due to their high saturation magnetization ($M_s = 16 \text{ kG}$), large energy product ($H_c M_s = 64 \text{ MGOe}$) and relatively low cost compared with that of $\text{Sm}_2\text{Fe}_{17}\text{N}_x$ ³. Furthermore, although the Curie temperature (T_C) is 592 K for $\text{Nd}_2\text{Fe}_{14}\text{B}$, the $\text{Nd}_2\text{Fe}_{14}\text{B}$ phase does not decompose until 1428 K, resulting in flexibility of its synthesis process. Therefore, $\text{Nd}_2\text{Fe}_{14}\text{B}$ and related compounds are widely used for high performance motors in many devices, electric vehicles and audio speakers.

In the ferromagnetic (FM) phase, past neutron scattering measurements suggested a collinear spin structure at room temperature⁴, in which both Fe and Nd moments (M_{Nd} & M_{Fe}) are aligned parallel along the $[001]$ direction. The magnitude of the ordered M_{Fe} was almost saturated even at 300 K, i.e. $\sim 2.2 \mu_B$, while M_{Nd} was initially thought to be below $1 \mu_B$ ⁴. The other neutron work reported that $M_{\text{Fe}} \sim 2.32(3) \mu_B$ and $M_{\text{Nd}} \sim 2.2 \mu_B$ ⁵, but the recent work revealed that $M_{\text{Fe}} = 1.9(1) \mu_B$ and $M_{\text{Nd}} = 1.5(1) \mu_B$ ⁶. Then, more detailed magnetization measurements at 4 K on $R_2\text{Fe}_{14}\text{B}$ with $R = \text{La}, \text{Y}, \dots$ revealed that $M_{\text{Fe}} = 2.1 \mu_B$ ², leading to $M_{\text{Nd}} = 3.2 \mu_B$. In addition, Nd-NMR measurements suggested that $M_{\text{Nd}} = 2.7 \mu_B$ at 4.2 K⁷. An X-ray magnetic circular dichroism (XMCD) study on $R_2\text{Fe}_{14}\text{B}$ ^{8,9} implied that the ordered M_R s are very close to the values obtained from gJ of $4f$ electrons, where J is the quantum number of the total angular momentum and g is the Landé factor. This means that $M_{\text{Nd}} \sim 3.3 \mu_B$.

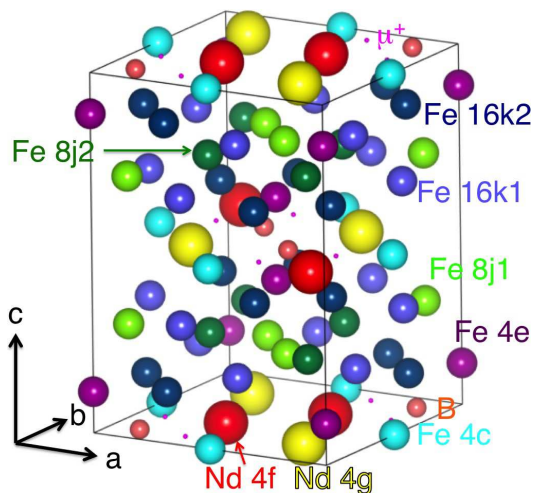


FIG. 1: The crystal structure of $\text{Nd}_2\text{Fe}_{14}\text{B}$ in tetragonal symmetry with space group $P4_2/mnm$ drawn by VESTA¹⁰. Large red and yellow spheres show Nd at two different sites, medium blue and green spheres show Fe at six different sites, and small orange spheres show B. Very small pink spheres represent the muon site (0.6744, 0.8840, 0) predicted by first principles calculations (see text).

Furthermore, the FM spin structure in $\text{Nd}_2\text{Fe}_{14}\text{B}$ was found to change at 135 K ($= T_{\text{SRT}}$) due to a spin re-orientation transition from a high-temperature phase with $\mathbf{M} \parallel [001]$ to a low-temperature phase with \mathbf{M} canted along the $[110]$ direction by magnetization measurements¹¹⁻¹⁴. Initially, a collinear FM structure with a canting angle $\theta = 30.6^\circ$ at 4.2 K was proposed based on magnetization measurements on a single crystal sample¹⁵, where θ is the angle of \mathbf{M} from the $[001]$ direction to the $[110]$ direction. However, both Mössbauer¹⁶

and XMCD¹⁷ measurements suggested a non-collinear spin structure below T_{SRT} . That is, $\theta_{\text{Fe}}^{\text{Möss}} = 27^\circ$ and $\theta_{\text{Nd}}^{\text{Möss}} = 58^\circ$ at 4.2 K, while $\theta_{\text{Fe}}^{\text{XMCD}} = 28^\circ$ and $\theta_{\text{Nd}}^{\text{XMCD}} = 40^\circ$ at 4.2 K. The continuation of XMCD work¹⁸ indicated the formation of a further noncollinear spin structure among the Nd moments at temperatures between 80 K and T_{SRT} , at which $\theta_{\text{Nd},4\text{f}} \sim 80^\circ$ and $\theta_{\text{Nd},4\text{g}} \sim 25^\circ$.

In order to further elucidate the FM ground state of $\text{Nd}_2\text{Fe}_{14}\text{B}$, we need another technique sensitive to internal magnetic field(s) (\vec{H}_{int}) in solids. Unfortunately, neutron scattering is unlikely to be useful for investigating the magnetic nature of ferromagnets, because relatively weak magnetic diffraction peaks always overlap with strong nuclear Bragg peaks. Indeed, the estimated M_{Nd} with neutron ranges from 1 to $2.2 \mu_{\text{B}}$ ⁴⁻⁶, which is rather small compared with those obtained with the other techniques. On the other hand, a positive muon spin rotation and relaxation ($\mu^+\text{SR}$) provides information on the local magnetic environments at the site(s) of the implanted muons, which usually locate at the interstitial site with the minimum electrostatic potential, regardless of magnetic order and/or disorder^{19,20}.

In fact, immediately after the discovery of the $\text{Nd}_2\text{Fe}_{14}\text{B}$ system, a $\mu^+\text{SR}$ experiment was performed at the Paul Sherrer Institut^{21,22} using powder $R_2\text{Fe}_{14}\text{B}$ samples with $R = \text{Y, Ce, Pr, Nd, Sm, Gd, Tb, Dy, Ho, Er, and Tm}$ in the temperature range between 300 and 4.2 K. The $\mu^+\text{SR}$ spectra obtained in zero external field (ZF) exhibited a clear oscillation with one precession frequency for all the samples, indicating both the formation of static FM order and a single muon lattice site. However, since it was very difficult to determine the correct muon site(s) in the lattice, the muon site was assumed to be a tetrahedral site with two Fe and two Nd nearest neighbors, based on the Mössbauer and neutron data of hydrated $R_2\text{Fe}_{14}\text{B}$ ^{22,23}. In addition, the lack of information on the local spin density at the muon site made it eventually impossible to estimate the magnitude of M_R . As a result, the past $\mu^+\text{SR}$ result is unlikely to be recognized as a crucial work for elucidating the magnetic ground state of $\text{Nd}_2\text{Fe}_{14}\text{B}$ and $R_2\text{Fe}_{14}\text{B}$.

We have therefore attempted to measure the $\mu^+\text{SR}$ spectra for $\text{Nd}_2\text{Fe}_{14}\text{B}$ up to above T_C to know the variation of H_{int} with temperature and to predict muon site(s) in the lattice with density functional theory (DFT) calculations. Using the predicted muon site and the measured local spin density at the muon site, the magnitude of M_{Nd} was clearly estimated even below T_{SRT} . Furthermore, using the past $\mu^+\text{SR}$ data for $R_2\text{Fe}_{14}\text{B}$ and the predicted muon site, we have obtained a systematic change in M_R with the number of 4f electrons in R .

II. EXPERIMENTAL

Aligned sintered plates of $\text{Nd}_2\text{Fe}_{14}\text{B}$ were prepared from jet-milled fine powder with the composition of 31.8Nd-0.98B-0.10Cu-0.90Co-0.15Al-0.05Ga-

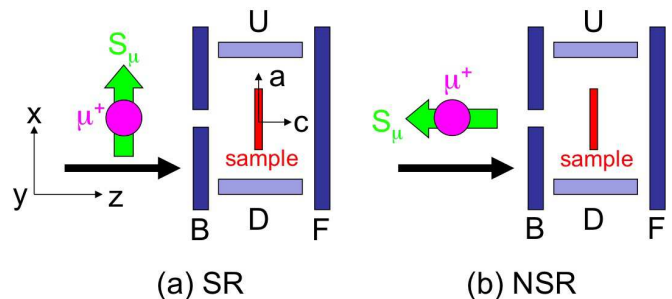


FIG. 2: (Color online) Geometry of the $\mu^+\text{SR}$ experiment in TRIUMF: four counters [backward (B), forward (F), up (U) and down (D)] detect decay positrons emitted in the $-z$, $+z$, $+x$ and $-x$ directions, respectively. The initial muon spin direction $\mathbf{S}_\mu(0)$ is in the $+x$ direction ($\parallel \hat{\mathbf{a}}$ of the plates) for spin-rotated (SR) mode (a) or in the $-z$ direction ($\parallel \hat{\mathbf{c}}$) for non-spin-rotated (NSR) mode (b). Thus if the internal magnetic field (\mathbf{H}_{int}) is parallel to $\hat{\mathbf{c}}$, only U and D counters will detect a muon spin oscillation, and that only in SR mode; but if $\mathbf{H}_{\text{int}} \perp \hat{\mathbf{c}}$, only B and F counters in NSR mode will show an oscillatory signal. Using both configurations, one can estimate the magnetic anisotropy in the sample.

66.02Fe (wt%). The mean particle size of the powder was about $6 \mu\text{m}$. The powders were then pressed under a magnetic field of 1.8 T followed by uniaxial pressing with 15 MPa. The pressed powders were sintered at 1293-1353 K for 4 hours in vacuum ($< 10^{-2}$ Pa). Finally, the sintered powder $8 \times 8 \times 8 \text{ mm}^3$ cube was sliced into 1 mm thick plates with the aligned c -axis perpendicular to the plane. The preparation and characterization of the sintered sample are explained in more detail elsewhere²⁴.

The $\mu^+\text{SR}$ time spectra were measured on the M20 surface muon beam line using the LAMPF spectrometer of the CMMS facility at TRIUMF in Canada. Four plates with $8 \times 8 \times 1 \text{ mm}^3$ were arranged onto a sample holder with their $\hat{\mathbf{c}}$ axes parallel to the beam direction (z) as defined in Fig. 2. For measurements in the T range between 1.8 and 300 K, the samples were attached to a low-background sample holder in a liquid-He flow-type cryostat with 0.05 mm thick Al-coated Mylar tape. For measurements in the T range between 300 and 600 K, the samples were fixed onto a silver plate by a 50 μm thick titanium foil, which is sandwiched between a second silver plate with a $16 \times 16 \text{ mm}^2$ square aperture through which incoming muons passed. For the former setup, there is essentially no background signal, while for the latter case the $\mu^+\text{SR}$ signal naturally includes a background signal from muons stopped in the surrounding silver plate.

The $\mu^+\text{SR}$ spectra were obtained in either zero applied field (ZF) or transverse field (TF) with four positron detectors [backward (B), forward (F), up (U) and down (D)] arranged as shown in Fig. 2. The initial direction of the muon polarization [$\mathbf{S}_\mu(0)$] relative to the plane of the plates was set by a Wien filter spin rotator. Here TF means the applied field is perpendicular to $\mathbf{S}_\mu(0)$, *i.e.* TF $\parallel y$ in this study. The experimental techniques are described in more detail elsewhere^{19,20}. The resulting

μ^+ SR data were analyzed with musrfit²⁵.

The distributions of electrostatic potential and local spin density were predicted by DFT calculations with a generalized gradient approximation (GGA) plus on-site Coulomb interaction (U), as described in Sec. III B.

III. RESULTS

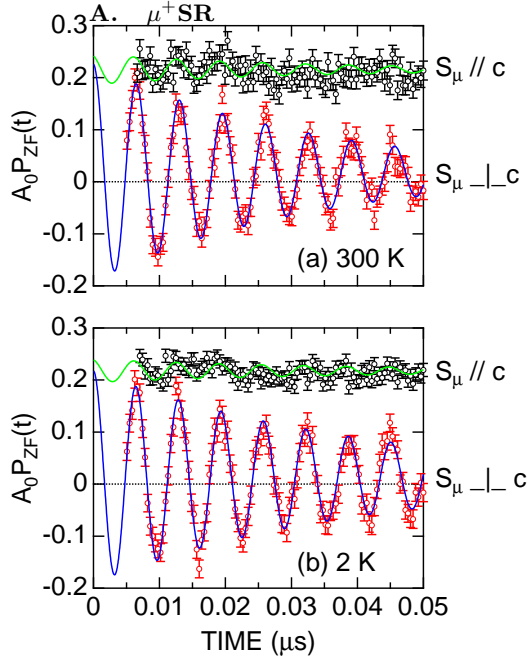


FIG. 3: (color online) The ZF- μ^+ SR spectrum for the sintered align $\text{Nd}_2\text{Fe}_{14}\text{B}$ plate sample recorded at (a) 300 K and (b) 2 K in two different configurations: a non-spin-rotated (NSR) mode [$\mathbf{S}_\mu(0) \parallel \hat{c}$] shown in red and a spin-rotated (SR) mode [$\mathbf{S}_\mu(0) \perp \hat{c}$] shown in green. The solid lines represent the best fits using Eq. (1).

Figure 3 shows the ZF- μ^+ SR time spectra for the $\text{Nd}_2\text{Fe}_{14}\text{B}$ sample recorded at 300 and 2 K. The spectrum obtained with SR mode [$\mathbf{S}_\mu \perp \hat{c}$] exhibits a clear oscillation, while that obtained with NSR mode [$\mathbf{S}_\mu \parallel \hat{c}$] shows mainly a non-oscillatory relaxation together with an oscillation with a very small amplitude. Since the Fourier transform frequency spectrum of the ZF- μ^+ SR time spectrum shows the presence of only one component, the two spectra were fitted by a combination of an exponentially relaxing cosine signal and an exponentially relaxing non-oscillatory signal:

$$A_0 P_{\text{ZF}}(t) = A_{\text{FM}} \exp(-\lambda_{\text{FM}} t) \cos(\omega_{\text{FM}} t + \phi_{\text{FM}}) + A_{\text{tail}} \exp(-\lambda_{\text{tail}} t). \quad (1)$$

Here A_0 is the initial asymmetry, $P_{\text{ZF}}(t)$ is the muon

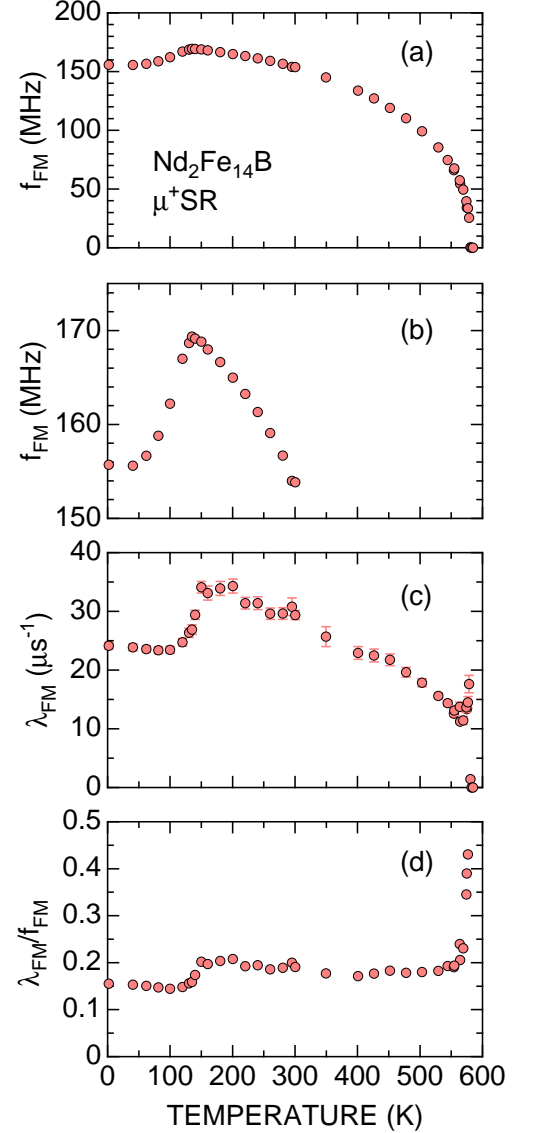


FIG. 4: (color online) The temperature dependences of (a) the muon spin precession frequency (f_{FM}), (b) the magnification of the $f_{\text{FM}}(T)$ curve to show the anomaly at around 135 K, (c) the exponential relaxation rate (λ_{FM}), and (d) the ratio between λ_{FM} and f_{FM} for the $\text{Nd}_2\text{Fe}_{14}\text{B}$ sample. The data were obtained by fitting the ZF- μ^+ SR spectrum with Eq. (1).

spin depolarization function in ZF, A_{FM} and A_{tail} are the asymmetries associated with the two signals, λ_{FM} and λ_{tail} are their exponential relaxation rates, $f_{\text{FM}} (\equiv \omega_{\text{FM}}/2\pi)$ is the muon Larmor frequency corresponding to the quasi-static internal FM field, and ϕ_{FM} is the initial phase. At each temperature, the two spectra were fitted using common λ_{FM} and f_{FM} .

Such fits yielded $A_{\text{FM}}^{\perp c} = 0.208(7)$, $A_{\text{FM}}^{\parallel c} = 0.021(5)$, $\lambda_{\text{FM}} = 30.6(1.3) \mu\text{s}^{-1}$, $f_{\text{FM}} = 153.3(2) \text{ MHz}$, $\phi_{\text{FM}}^{\perp c} =$

1(2) deg, $\phi_{\text{FM}}^{S\parallel c} = 10(14)$ deg, $A_{\text{tail}}^{S\perp c} = 0.0159(2)$, $A_{\text{tail}}^{S\parallel c} = 0.2160(4)$, and $\lambda_{\text{tail}} = 0.0141(6) \mu\text{s}^{-1}$ at 300 K. Thus, the deviation from the c -axis of the magnetic field at the muon site, i.e. the magnetic anisotropy at the muon site is estimated to be $\Theta(300 \text{ K}) = \tan^{-1} \left(A_{\text{FM}}^{S\parallel c} / A_{\text{FM}}^{S\perp c} \right) = 7(4)$ deg. The same fit to the data at 2 K yielded $\Theta(2 \text{ K}) = 6(4)$ deg. This means that Θ is almost zero below 250 K within the accuracy of $\mu^+\text{SR}$.

Figure 4 shows the temperature dependences of f_{FM} , λ_{FM} , and $\lambda_{\text{FM}}/f_{\text{FM}}$ for the $\text{Nd}_2\text{Fe}_{14}\text{B}$ sample. The $f_{\text{FM}}(T)$ curve exhibits an order parameter-like temperature dependence and f_{FM} disappears at temperatures above around 582 K ($= T_C^{\mu\text{SR}}$), which is slightly lower than T_C in literatures, *i.e.* 592 K^{1,2}. Here it should be noted that $T_C^{\mu\text{SR}}$ is estimated from the data obtained in ZF, while the other techniques require the application of a large external magnetic field, which naturally enhances FM order. The $f_{\text{FM}}(T)$ curve also shows a sharp local maximum at 135 K ($= T_{\text{SRT}}$), indicating a change in the local FM environment caused by a spin reorientation transition.

As temperature increases from 2 K, λ_{FM} decreases slightly up to 100 K, then suddenly increases up to 150 K, and then decreases again towards T_C with an increasing slope ($d\lambda_{\text{FM}}/dT$). However, below the vicinity of T_C , λ_{FM} rapidly increases with temperature, and then suddenly drops to zero at T_C ; that is, a critical behavior is observed below the vicinity of T_C .

It should be noted that $\lambda_{\text{FM}}/f_{\text{FM}}$, which corresponds to the normalized field distribution width, is almost temperature independent at temperatures below 100 K and at temperatures between 150 and 550 K. This means that besides the temperatures around a spin reorientation transition and below the vicinity of T_C , H_{int} in the FM phase depends only on the magnitude of the ordered moments. These results suggest that muons are stable in the $\text{Nd}_2\text{Fe}_{14}\text{B}$ lattice until $T_C^{\mu\text{SR}}$. The present result reproduces those in past $\mu^+\text{SR}$ work carried out below room temperature^{21,22}.

In order to estimate T_C more correctly, Fig. 5 shows the temperature dependence of the weak transverse asymmetry (A_{TF}) measured with $\text{TF}=50$ Oe in the vicinity of T_C , together with that of f_{FM} . Here, “weak” means that the applied TF is very small compared with H_{int} caused by FM order. The wTF- $\mu^+\text{SR}$ spectrum was fitted by a combination of an exponentially relaxing cosine oscillation due to muon spin precession in TF and Eq. (1):

$$\begin{aligned} A_0 P_{\text{TF}}(t) = & A_{\text{TF}} \exp(-\lambda_{\text{TF}}t) \cos(\omega_{\text{TF}}t + \phi_{\text{TF}}) \\ & + A_{\text{FM}} \exp(-\lambda_{\text{FM}}t) \cos(\omega_{\text{FM}}t + \phi_{\text{FM}}) \\ & + A_{\text{tail}} \exp(-\lambda_{\text{tail}}t). \end{aligned} \quad (2)$$

At temperatures $T \gg T_C$, $A_{\text{FM}} = A_{\text{tail}} = 0$; at temperatures $T \ll T_C$, $A_{\text{TF}} = 0$. From the middle point of a step-like change in the $A_{\text{TF}}(T)$ curve, T_C is estimated as 581.57(14) K, because A_{TF} is proportional to the volume fraction of paramagnetic phases in a sample. The finite value of A_{TF} below T_C (~ 0.06) is from muons stopped

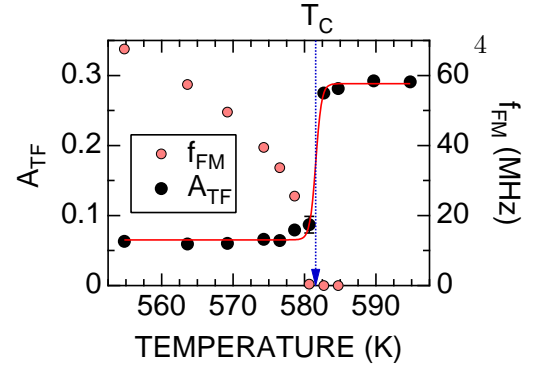


FIG. 5: (color online) The temperature dependences of f_{FM} and the weak transverse field asymmetry (A_{TF}) with $\text{TF}=50$ Oe. The $f_{\text{FM}}(T)$ curve is the same as that in Fig. 4(a). Here T_C corresponds to the midpoint of a step-like change in the $A_{\text{TF}}(T)$ curve.

in the surrounding silver plate.

B. DFT calculations

First-principles calculations based on a density functional theory (DFT)^{26,27} have been performed to determine the muon site in $\text{Nd}_2\text{Fe}_{14}\text{B}$. A self consistent field (SCF) calculation is carried out using the ultrasoft pseudopotential method^{28,29}, where the on-site Coulomb interaction for localized Nd-4*f* electrons is taken into consideration using the DFT + *U* method^{30,31}. The obtained pseudo SCF charge density is transformed into an all electron form with the projector augmented wave operators³², from which the muon occupation site is estimated by the electrostatic potential analysis. The program used for the DFT calculations is an original code developed by one of the authors (K. M.), which has been successfully applied for various materials³³⁻³⁷.

The cutoff energies of plane waves are set to be 25 and 200 hartrees for the pseudo wavefunctions and the charge density, respectively. The $4 \times 4 \times 4$ k -point mesh is adopted for the Brillouin zone integration. The generalized gradient approximation³⁸ is used for the exchange-correlation functional. The effective Coulomb and exchange parameters for Nd-4*f* orbitals are assumed to be $U = 5$ eV³⁹ and $J = 0.5$ eV, respectively.

Table I shows the result of the structural relaxation in which atomic positions as well as lattice constants are fully optimized. The calculated parameters are in good agreement with the experimental ones⁴⁰. Figure 6(a) depicts the electrostatic potential: The muon site is found to be $8i$ (0.6745, 0.8838, 0) which is located near the center of a square base of a pyramid composed of Nd-3Fe-B atoms. As shown in Fig. 6(b), the spin density at the muon site is negligibly small, $\rho_{\text{spin}} = -2 \times 10^{-3} \mu_B/\text{bohr}^3$, which is eventually zero. It

should be noted that the DFT calculations with $U = 0$ provides very similar muon site and local spin density to those predicted with $U = 5$ eV. This means that the two significant parameters, i.e. the muon site and ρ_{spin} , are not sensitive to U in the $\text{Nd}_2\text{Fe}_{14}\text{B}$ lattice.

TABLE I: Crystallographic parameters of ferromagnetic $\text{Nd}_2\text{Fe}_{14}\text{B}$. Space group: $P4_2/mnm$ (No. 136). Lattice constants: $a = 8.797$ Å, $c = 12.149$ Å (Calc.), and $a = 8.795$ Å, $c = 12.188$ Å (Expt.).

site	Calc.			Expt. ^a			
	x	y	z	x	y	z	
Nd1	4 <i>g</i>	0.2313	0.7687	0	0.2313	0.7687	0
Nd2	4 <i>f</i>	0.3570	0.3570	0	0.3585	0.3585	0
Fe1	16 <i>k</i>	0.0373	0.3599	0.3239	0.0379	0.3587	0.3237
Fe2	16 <i>k</i>	0.0675	0.2754	0.1270	0.0671	0.2765	0.1269
Fe3	8 <i>j</i>	0.0980	0.0980	0.2950	0.0979	0.0979	0.2951
Fe4	8 <i>j</i>	0.3180	0.3180	0.2542	0.3174	0.3174	0.2535
Fe5	4 <i>e</i>	0	0	0.1143	0	0	0.1144
Fe6	4 <i>c</i>	0	1/2	0	0	1/2	0
B	4 <i>f</i>	0.1236	0.1236	0	0.1243	0.1243	0

^aReference⁴⁰

On the contrary, the ordered magnetic moment of each element varies with U (Table II). More correctly, the introduction of $U = 5$ eV reduces M_{Nd} by 10%, while the change in M_{Fe} is about 1%. The magnitude of M_{Fe} at each site is comparable to the reported ones (see Table III). This indicates the importance of the magnitude of U for estimating M_{Nd} by DFT calculations.

TABLE II: The ordered magnetic moment of each element in $\text{Nd}_2\text{Fe}_{14}\text{B}$ predicted by DFT calculations without and with $U = 5$ eV.

site	GGA	GGA+ U	
	M (μ_{B})	M (μ_{B})	
Nd1	4 <i>g</i>	2.92	2.74
Nd2	4 <i>f</i>	3.01	2.72
Fe1	16 <i>k</i>	2.25	2.28
Fe2	16 <i>k</i>	2.20	2.22
Fe3	8 <i>j</i>	2.09	2.17
Fe4	8 <i>j</i>	2.68	2.68
Fe5	4 <i>e</i>	2.03	2.03
Fe6	4 <i>c</i>	2.32	2.36
B	4 <i>f</i>	-0.25	-0.26

IV. DISCUSSION

A. $\text{Nd}_2\text{Fe}_{14}\text{B}$

For non-magnetized ferromagnetic materials in zero applied field, the internal magnetic field at a muon site (\mathbf{H}_{μ}) is represented by^{20,41-43};

$$\mathbf{H}_{\text{FM}} = \mathbf{H}_{\mu}$$

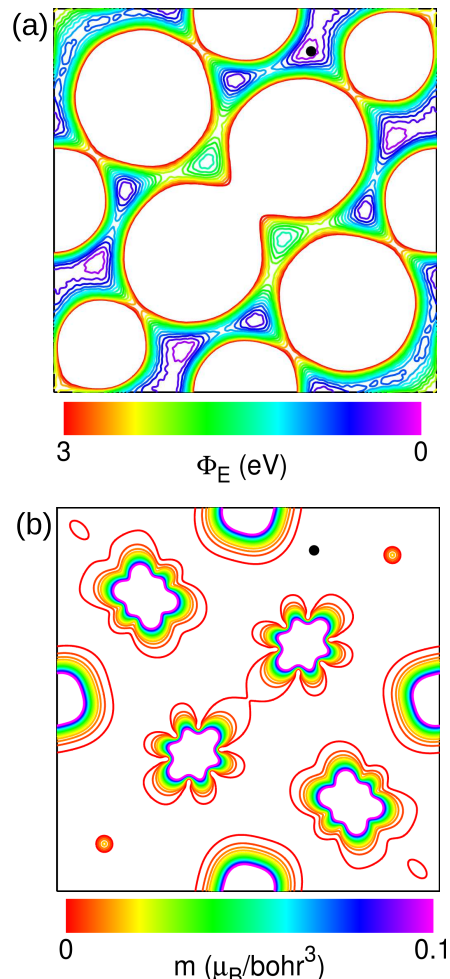


FIG. 6: Contour plots for $\text{Nd}_2\text{Fe}_{14}\text{B}$ in the (001) plane. (a) Electrostatic potential Φ_{E} and (b) spin density $m (= \rho^{\uparrow} - \rho^{\downarrow})$. The muon site is indicated by black circles.

$$= \mathbf{H}_{\text{dip}} + \mathbf{H}_{\text{L}} + \mathbf{H}_{\text{hf}}, \quad (3)$$

This field is connected to the muon-spin precession frequencies through the muon gyromagnetic ratio [$f = H\gamma_{\mu}/(2\pi) = 0.013553$ (MHz/Oe) $\times H$ (Oe)] leading to

$$\begin{aligned} f_{\text{FM}} &= f_{\mu} \\ &= f_{\text{dip}} + f_{\text{L}} + f_{\text{hf}} \end{aligned} \quad (4)$$

where \mathbf{H}_{dip} is the dipolar field, \mathbf{H}_{L} is the Lorentz field, \mathbf{H}_{hf} is the hyperfine field, and f_{μ} , f_{L} , and f_{hf} are the corresponding muon spin precession frequencies. Furthermore, \mathbf{H}_{L} and \mathbf{H}_{hf} are connected to the saturated magnetization (\mathbf{M}_{s}) and the local spin density at the muon sites (ρ_{spin}) as follows:

$$\begin{aligned} \mathbf{H}_{\text{dip}} &= -\frac{1}{4\pi\mu_0} \nabla \left(\frac{\mathbf{m} \cdot \mathbf{r}}{r^3} \right), \\ \mathbf{H}_{\text{L}} &= \frac{4\pi}{3} \times \mathbf{M}_{\text{s}}, \end{aligned}$$

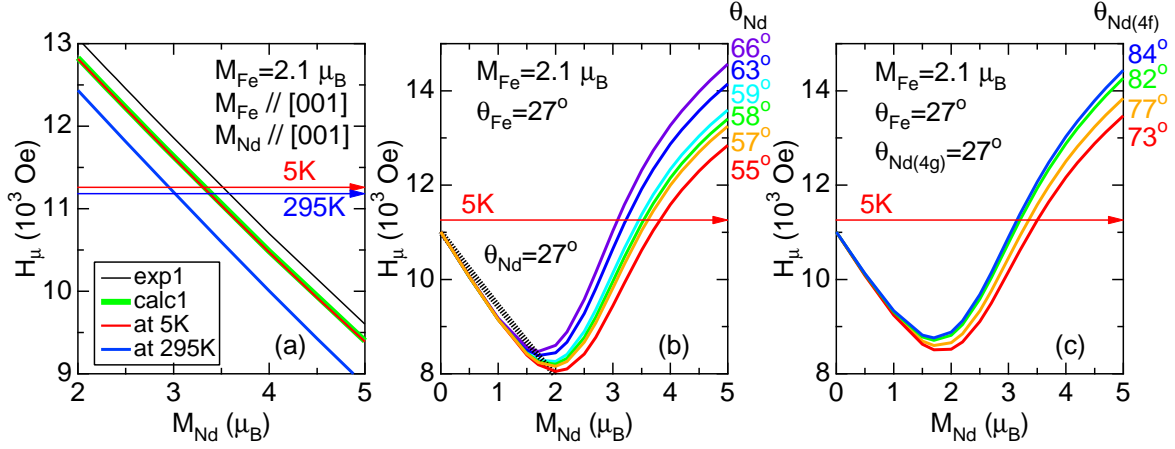


FIG. 7: The relationship between the calculated H_μ and M_{Nd} in $\text{Nd}_2\text{Fe}_{14}\text{B}$ using the model that (a) $\mathbf{M}_{\text{Fe}} \parallel [001]$ and $\mathbf{M}_{\text{Nd}} \parallel [001]$; (b) \mathbf{M}_{Fe} and \mathbf{M}_{Nd} are both canted from the $[001]$ direction to the $[110]$ direction with a canting angle (θ) of 27° for Fe and $55\text{--}66^\circ$ for Nd; and (c) $\theta = 27^\circ$ for Fe and Nd at the $4g$ site, but $\theta = 73\text{--}84^\circ$ for Nd at the $4f$ site. In (b), a collinear FM spin arrangement — *i.e.* $\theta_{\text{Fe}} = \theta_{\text{Nd}} = 27^\circ$ — is also shown with a broad black line.

$$\mathbf{H}_{\text{hf}} = \frac{8\pi}{3} \times \rho_{\text{spin}}(\mathbf{r}_\mu). \quad (5)$$

In order to estimate \mathbf{H}_{dip} (f_{dip}), we use the results of neutron diffraction⁴ and Mössbauer⁴⁴ measurements for the magnitude and direction of the Fe moments. Assuming that the magnitude of the ordered M_{Fe} is $2.1 \mu_{\text{B}}^2$, \mathbf{H}_{dip} at the muon site is easily calculated as a function of the Nd moment using crystal structural data with *dipelec*⁴⁵.

We start by considering a collinear FM structure along the c -axis, that is, $\mathbf{M}_{\text{Fe}} \parallel [001]$ and $\mathbf{M}_{\text{Nd}} \parallel [001]$. Since $4\pi M_s = 18.5 \text{ kOe}$ at 5 K (see Table IV)^{2,22}, $\mathbf{H}_{\text{L}} = (0, 0, 6.2 \text{ kOe})$ from Eq. (5). Moreover, $\mathbf{H}_{\text{hf}} = (0, 0, 0)$ because of the absence of any local spin density at the muon site. Consequently, we obtain the relationship between $|\mathbf{H}_\mu| = H_\mu^{\text{calc}}$ and the magnitude of the Nd moment (M_{Nd}), as seen in Fig. 7(a). Here, the measured value of f_μ (f_μ^{exp}) is $152.6(2) \text{ MHz}$ at 2.2 K, which is very close to the reported value (156 MHz) at 5 K. Thus, in order to explain H_μ^{exp} , M_{Nd} is uniquely determined as $3.31 \mu_{\text{B}}$. This is almost equivalent to M_{Nd} estimated from magnetization measurements, *i.e.* $M_{\text{Nd}} = 3.2 \mu_{\text{B}}^2$, confirming the reliability of the predicted muon site from DFT calculations. From the data at room temperature, *i.e.* $4\pi M_s = 16.0 \text{ kOe}$ at 295 K and $H_\mu^{\text{exp}} = 151(2) \text{ MHz}$ at 300 K, we also obtain that $M_{\text{Nd}} = 3.01 \mu_{\text{B}}$.

Although we assumed that $M_{\text{Fe}} = 2.1 \mu_{\text{B}}$, M_{Nd} estimated with the above procedure is found to increase linearly with M_{Fe} (see Fig. 8). On the contrary, Fig. 8 provides an acceptable range for M_{Fe} as $2.0 \leq M_{\text{Fe}} \leq 2.15 \mu_{\text{B}}$, when M_{Nd} ranges between 3.0 and $3.5 \mu_{\text{B}}$. Furthermore, we assumed that M_{Fe} is identical for all the Fe sites. However, experimental studies and DFT calculations reported that M_{Fe} at each site deviates slightly from $2.1 \mu_{\text{B}}$. In order to know the effect of such deviations on the estimation of M_{Nd} , the relationship between H_μ and M_{Nd} is also shown for the two cases in Fig. 7(a) and six

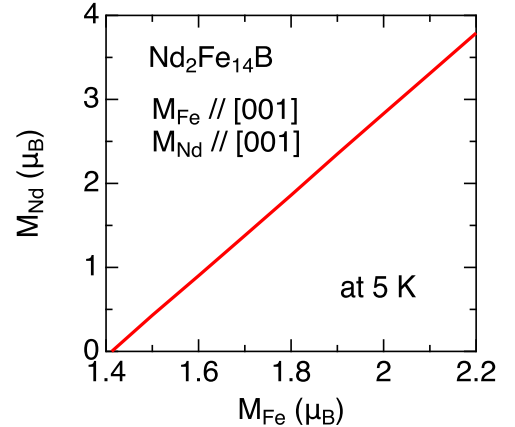


FIG. 8: The relationship between M_{Nd} and M_{Fe} in $\text{Nd}_2\text{Fe}_{14}\text{B}$ using the model that $\mathbf{M}_{\text{Fe}} \parallel [001]$ and $\mathbf{M}_{\text{Nd}} \parallel [001]$.

cases in Table III. This indicates that the four estimations for M_{Fe} , *i.e.* *exp2*, *exp3*, *calc2*, and *calc3*, provide unusually large M_{Nd} under the collinear FM structure along the c -axis.

By contrast, at low temperatures the spin orientation is reported to change from the $[001]$ to the $[110]$ direction below $T_{\text{SRT}} = 135 \text{ K}$ ^{11–14}. The corresponding anomaly is clearly seen in the $f_{\text{FM}}(T)$ and $\lambda_{\text{FM}}(T)$ curves [Fig. 4]. More correctly, both Fe and Nd moments are thought to be *canted* towards the $[110]$ direction from the $[001]$ direction, based on both first principles calculations and Fe K -edge x-ray magnetic circular dichroism (XMCD) measurements¹⁷. The canting angle (θ) was estimated to be 27° for Fe ($\theta_{\text{Fe}} = 27^\circ$) and 58° for Nd ($\theta_{\text{Nd}} = 58^\circ$) at 4.2 K. Figure 7(b) shows the relationship between H_μ and M_{Nd} for several θ_{Nd} values. The μ^+ SR result clearly

excludes a collinear structure, in which $\theta_{\text{Fe}} = \theta_{\text{Nd}} = 27^\circ$, as an FM ground state. On the other hand, non-collinear structures provide a more plausible M_{Nd} , particularly when $\theta_{\text{Nd}} \sim 60^\circ$. If we assume that $M_{\text{Nd}} = 3.2 \mu_{\text{B}}$, θ_{Nd} should be 63° , which is very close to the value reported by XMCD (58°).

Dipole field calculations provide that the magnetic anisotropy at the muon site (Θ) is 16 deg at temperatures below T_{SRT} , while $\Theta = 0$ deg at temperatures above T_{SRT} . Making comparison with the experimental result [$\Theta(300 \text{ K}) = 7(4)\text{deg}$ and $\Theta(2 \text{ K}) = 6(4)\text{deg}$], the experimental accuracy of Θ was likely to be overestimated. This is probably due to the fact that $\mathbf{S}_\mu(0)$ for NSR mode is deviated from the z direction by about 10 deg to eliminate the other particles in the muon beam. Nevertheless, we should note that the above estimation for M_{Nd} is based only on the magnitude of f_μ , and as a result, the estimated value is not affected by the alignment of the sample.

Another XMCD study at low temperatures¹⁸ proposed the possibility of a non-collinear spin arrangement among the Nd moments. That is, $\theta_{\text{Nd}} \sim 25^\circ$ for the Nd ions at the $4g$ site, but $\theta_{\text{Nd}} \sim 80^\circ$ for the Nd ions at the $4f$ site. Figure 7(c) shows the dependence of H_μ on M_{Nd} as $\theta_{\text{Nd}(4f)}$ changes from 73 to 84° . The calculations also predict that $\theta_{\text{Nd}} = 82^\circ$ for $M_{\text{Nd}} = 3.2 \mu_{\text{B}}$, which looks consistent with the proposed arrangement. However, we should note that there are eight crystallographically equivalent muon sites ($8i$) in the $\text{Nd}_2\text{Fe}_{14}\text{B}$ lattice. Moreover, such a non-collinear spin arrangement among the Nd moments produces two different $H_{\mu,s}$ at each $8i$ site — namely, $H_\mu = 11270 \text{ Oe}$ for four of the sites and 11655 Oe for the other four sites. Although the difference of the two $H_{\mu,s}$ (about 4%) is too small to observe two distinct muon precession frequencies in the ZF- μ^+ SR spectrum, such a split naturally increases the field distribution width, resulting in an increased relaxation rate λ_{FM} . In reality, λ_{FM} and $\lambda_{\text{FM}}/f_{\text{FM}}$ at 2 K are smaller than those at room temperature [Fig. 4(b)]. This clearly excludes the model of a non-collinear spin arrangement among the Nd moments from the FM ground state for $\text{Nd}_2\text{Fe}_{14}\text{B}$. Since the $\lambda_{\text{FM}}(T)$ curve exhibits a broad maximum at around T_{SRT} [see Fig. 4(b)], such a non-collinear spin arrangement among the Nd moments could appear in a limited temperature range particularly below the vicinity of T_{SRT} . Even for this case, the predicted Θ is the same to that for the collinear spin arrangement among the Nd moments, i.e. 16 deg. Therefore, Θ provides no crucial information on the spin arrangement in $\text{Nd}_2\text{Fe}_{14}\text{B}$ within the present accuracy.

B. $R_2\text{Fe}_{14}\text{B}$

Although we have measured μ^+ SR spectra only for $\text{Nd}_2\text{Fe}_{14}\text{B}$, both \mathbf{H}_μ and \mathbf{M}_s were reported for the other $R_2\text{Fe}_{14}\text{B}$ compounds with $R = \text{Y, Ce, Pr, Sm, Gd, Tb, Dy, Ho, Er, and Tm}$ (see Table IV)^{21,22}. Since $4f$ elec-

trons are well localized at the R site, it is reasonable to assume the same muon site in $R_2\text{Fe}_{14}\text{B}$ as in $\text{Nd}_2\text{Fe}_{14}\text{B}$. Concerning the spin arrangement in the FM phase, the easy direction of magnetization at base temperature² revealed that both \mathbf{M}_{Fe} and \mathbf{M}_R are parallel to the $[001]$ direction in $R_2\text{Fe}_{14}\text{B}$ with $R = \text{Y, Ce, Pr, Nd, Gd, Tb, Dy, and Ho}$, but they are parallel to the $[100]$ direction in $R_2\text{Fe}_{14}\text{B}$ with $R = \text{Sm, Er, and Tm}$. We also assume that $M_{\text{Fe}} = 2.1 \mu_{\text{B}}$ in $R_2\text{Fe}_{14}\text{B}$ regardless of R .

Using the structural data of each compound, Fig. 9 shows the relationship between H_μ and M_R . For $\text{Y}_2\text{Fe}_{14}\text{B}$, M_{Y} is estimated to be almost zero ($0.11 \mu_{\text{B}}$), as expected for Y^{3+} . In fact, the recent photoelectron spectroscopic analysis result on $\text{Nd}_2\text{Fe}_{14}\text{B}$ ^{51,52} revealed that the valence state of Nd ions is very close to $3+$, while there is, to our knowledge, no XPS work on $\text{Y}_2\text{Fe}_{14}\text{B}$. As the atomic number increases, H_μ^{exp} decreases systematically. From the intersection between H_μ^{exp} and H_μ^{calc} , M_{Ce} and M_{Pr} are estimated to be 0.66 and $2.79 \mu_{\text{B}}$, respectively (Table IV).

For $\text{Sm}_2\text{Fe}_{14}\text{B}$, $\text{Er}_2\text{Fe}_{14}\text{B}$, and $\text{Tm}_2\text{Fe}_{14}\text{B}$, since $\mathbf{M}_{\text{Fe}} \parallel [100]$ and $\mathbf{M}_R \parallel [100]$, the $H_\mu^{\text{calc}}(M_R)$ curve exhibits a parabolic shape with a minimum at $M_R = 0$ [Fig. 9(b)]. For $\text{Sm}_2\text{Fe}_{14}\text{B}$, $H_\mu^{\text{exp}} < H_\mu^{\text{calc}}$ in the whole possible range of M_{Sm} , leading tentatively to $M_{\text{Sm}} = 0$. This implies that the FM spin structure is slightly different from the proposed one⁵³. For $\text{Er}_2\text{Fe}_{14}\text{B}$, and $\text{Tm}_2\text{Fe}_{14}\text{B}$, there are two intersections between the $H_\mu^{\text{exp}}(M_R)$ and $H_\mu^{\text{calc}}(M_R)$ curves. This means that two values are available for M_{Er} and M_{Tm} . However, neutron diffraction measurements proposed that \mathbf{M}_R is antiparallel to \mathbf{M}_{Fe} ^{54–56}. Therefore, a negative value is selected for M_{Er} and M_{Tm} , that is, -9.94 and $-9.54 \mu_{\text{B}}$, respectively.

For $\text{Gd}_2\text{Fe}_{14}\text{B}$ ², $\text{Tb}_2\text{Fe}_{14}\text{B}$ ⁵⁷, $\text{Dy}_2\text{Fe}_{14}\text{B}$ ⁵⁸, and $\text{Ho}_2\text{Fe}_{14}\text{B}$ ⁵⁹, $\mathbf{M}_{\text{Fe}} \parallel [001]$, $\mathbf{M}_R \parallel [001]$, and \mathbf{M}_R is antiparallel to \mathbf{M}_{Fe} . Indeed, H_μ^{exp} is reproduced only when $M_R < -9 \mu_{\text{B}}$ [Fig. 9(c)]. As a result, we obtain that $M_{\text{Gd}} = -9.48 \mu_{\text{B}}$, $M_{\text{Tb}} = -11.4 \mu_{\text{B}}$, $M_{\text{Dy}} = -12.6 \mu_{\text{B}}$, and $M_{\text{Ho}} = -10.3 \mu_{\text{B}}$.

Finally, Fig. 10 shows the relationship between M_R and the expected magnetic moment (gJ) derived from Landé g factor and the quantum number of the total angular momentum (J) for free R^{3+} ions. M_R estimated with the magnetization measurements (M_R^{Mag}) is almost equivalent to gJ^2 , suggesting the presence of stronger exchange field to the $4f$ moments than the crystal field². On the other hand, the slope of the $M_R^{\mu\text{SR}}(gJ)$ curve estimated with μ^+ SR is steeper than that for the $M_R^{\text{Mag}}(gJ)$ curve, mainly because $|M_R^{\mu\text{SR}}| > |M_R^{\text{Mag}}|$ for the heavy rare earth elements. Although the reason for this discrepancy is not clear at present, we should note that μ^+ SR is very sensitive to local magnetic environments. Recently, not only for $\text{Nd}_2\text{Fe}_{14}\text{B}$ but also for $\text{Ho}_2\text{Fe}_{14}\text{B}$, a non-collinear spin structure for the Ho moment is proposed with neutron using a single crystal sample⁵⁹. This implies the possibility that such non-collinear structure appears in the other $R_2\text{Fe}_{14}\text{B}$ at low temperatures, which

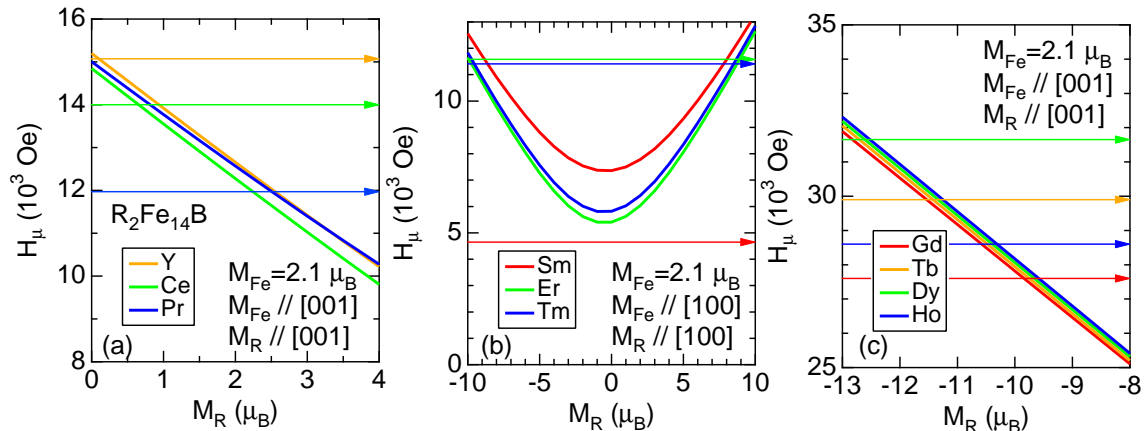


FIG. 9: The relationship between the calculated H_μ and M_{Nd} in $R_2Fe_{14}B$ using the model that (a) $M_{Fe} \parallel [001]$ and $M_R \parallel [001]$, (b) $M_{Fe} \parallel [100]$ and $M_R \parallel [100]$, and (c) $M_{Fe} \parallel [001]$ and $M_R \parallel [001]$. In (a)-(c), the magnitude of M_{Fe} is assumed to be $2.1 \mu_B$.

TABLE III: The Fe moment at each site in $Nd_2Fe_{14}B$ and the Nd moment (M_{Nd}) estimated from the μ^+SR data.

case	16k1	16k2	8j1	8j2	4e	4c	average	M_{Nd}
average	2.1	2.1	2.1	2.1	2.1	2.1	2.1	3.31
exp1 ⁴⁶	2.08	2.16	2.06	2.43	2.28	1.97	2.16	3.52
exp2 ¹⁶	2.24	2.30	2.21	2.55	2.00	2.17	2.28	4.27
exp3 ⁴⁷	2.27	2.41	2.19	2.70	2.20	2.10	2.38	4.61
calc1 ⁴⁸	2.15	2.18	2.12	2.74	2.13	1.59	2.20	3.33
calc2 ⁴⁹	2.22	2.28	2.67	2.16	1.96	2.43	2.29	3.80
calc3 ⁵⁰	2.28	2.37	2.32	2.74	2.19	2.46	2.38	4.27

would affect the magnitude of $M_R^{\mu SR}$. It would be thus an interesting subject to reconfirm the magnetic structure in $R_2Fe_{14}B$ at low temperatures using a high quality sample. Finally, this work clearly demonstrates the unique power of a combination of μ^+SR and DFT calculations for determining the magnetic moments of rare earth elements through the observation of local H_{int} .

V. SUMMARY

We have studied the internal magnetic field in a sintered $Nd_2Fe_{14}B$ permanent magnet sample with a positive muon spin rotation and relaxation (μ^+SR) technique, which provides microscopic magnetic information at the muon site. Combining the μ^+SR data with the result of DFT calculations for predicting the muon site in the lattice, the magnitude of the ordered Nd moment was clearly estimated both for a collinear ferromagnetic structure at room temperature and a canted

ferromagnetic structure at 2 K. Furthermore, a similar estimation for the ordered moment of the rare earth elements in $R_2Fe_{14}B$ provided reasonable values consistent with those reported by magnetization and Mössbauer measurements. μ^+SR has been widely used for investigating a magnetic nature in antiferromagnetic, spin-glass, and/or paramagnetic materials, in which both the Lorentz field and hyperfine field are usually zero and, as a result, the dipole field is predominant. On the contrary, the present work demonstrates that a combination of μ^+SR and DFT calculations further expands the research field into ferromagnetic materials.

VI. ACKNOWLEDGMENTS

We thank the staff of TRIUMF (especially the CMMS) for help with the μ^+SR experiments. This work was supported by Japan Society for the Promotion Science (JSPS) KAKENHI Grant No. JP18H01863.

* Electronic address: juns@triumf.ca; Present address: CROSS Neutron Science and Technology Center, Tokai,

Ibaraki 319-1106, Japan
¹ M. Sagawa, S. Fujimura, N. Togawa, H. Yamamoto, and

TABLE IV: The internal magnetic field detected with μ^+SR^{22} , the saturated magnetization², the magnetic moment of R (M_R) estimated with μ^+SR ($M_R^{\mu SR}$), and M_R proposed with magnetization measurements at 4 K (M_R^{Mag})², and gJ , where g is the Landé g -factor and J is the quantum number of the total angular momentum.

$R_2Fe_{14}B$	H_μ (MHz)	H_μ (kOe)	$3H_L = 4\pi M_s$ (kOe)	$M_R^{\mu SR}$ (μ_B)	M_R^{Mag} (μ_B)	gJ
$R = Y$	204.5	15.07	15.9	0.11	0	—
La	—	—	14.8	—	—	0
Ce	189.6	14.0	14.7	0.66	—	2.14
Pr	162.5	11.97	18.4	2.79	3.1	3.20
Nd	152.6	11.26	18.5	3.31	3.2	3.27
Pm	—	—	—	—	—	2.40
Sm	63.0	4.65	16.7	~ 0	1.0	0.72
Eu	—	—	—	—	—	0
Gd	374.0	27.60	9.2	-9.48	-6.8	7.0
Tb	405.2	29.90	6.6	-11.4	-9.1	9.0
Dy	429.0	31.65	5.7	-12.6	-10.1	10.0
Ho	388.0	28.60	5.7	-10.3	-10.1	10.0
Er	157.2	11.58	6.6	-9.94	-9.3	9.0
Tm	154.6	11.41	9.2	-9.57	-6.7	7.0
Yb	—	—	~ 12	—	-4.2	4.0
Lu	—	—	14.7	—	—	0

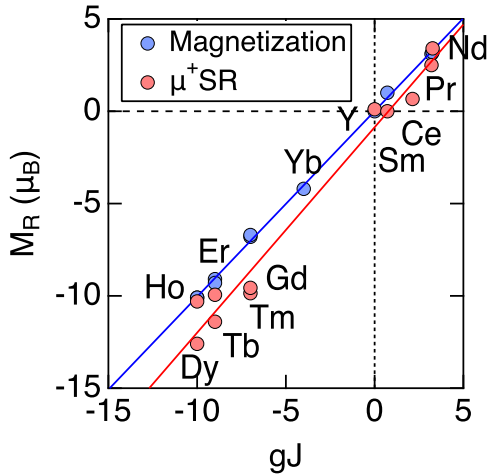


FIG. 10: The relationship between the magnetic moment of the rare earth element (M_R) and expected magnetic moments (gJ). For heavy rare earth elements, negative value of gJ is used, because M_R is antiparallel to M_{Fe} .

Y. Matsuura, Journal of Applied Physics **55**, 2083 (1984).

² J. F. Herbst, Rev. Mod. Phys. **63**, 819 (1991).

³ J. Coey and H. Sun, Journal of Magnetism and Magnetic Materials **87**, L251 (1990).

⁴ J. F. Herbst, J. J. Croat, F. E. Pinkerton, and W. B. Yelon, Phys. Rev. B **29**, 4176 (1984).

⁵ D. Givord, H. S. Li, and F. Tasset, Journal of Applied Physics **57**, 4100 (1985).

⁶ A. Teplykh, Y. Chukalkin, S. Lee, S. Bogdanov, N. Kudrevatykh, E. Rosenfeld, Y. Skryabin, Y. Choi, A. Andreev, and A. Pirogov, Journal of Alloys and Compounds **581**, 423 (2013).

⁷ E. Potenziani II, Journal of Applied Physics **58**, 2764

(1985).

⁸ J. Chaboy, H. Maruyama, L. M. García, J. Bartolomé, K. Kobayashi, N. Kawamura, A. Marcelli, and L. Bozukov, Phys. Rev. B **54**, R15637 (1996).

⁹ J. Miguel-Soriano, J. Chaboy, L. M. Garcia, F. Bartolome, and H. Maruyama, Journal of Applied Physics **87**, 5884 (2000).

¹⁰ K. Momma and F. Izumi, J. Appl. Cryst. **41**, 653 (2008).

¹¹ D. Givord, H. Li, and R. P. de la Bathie, Solid State Communications **51**, 857 (1984).

¹² C. Abache and H. Oesterreicher, Journal of Applied Physics **57**, 4112 (1985).

¹³ M. Sagawa, S. Fujimura, H. Yamamoto, Y. Matsuura, and S. Hirosawa, Journal of Applied Physics **57**, 4094 (1985).

¹⁴ S. Hirosawa, Y. Matsuura, H. Yamamoto, S. Fujimura, M. Sagawa, and H. Yamauchi, Journal of Applied Physics **59**, 873 (1986).

¹⁵ K. Tokuhara, Y. Ohtsu, F. Ono, O. Yamada, M. Sagawa, and Y. Matsuura, Solid State Communications **56**, 333 (1985).

¹⁶ H. Onodera, H. Yamauchi, M. Yamada, H. Yamamoto, M. Sagawa, and S. Hirosawa, Journal of Magnetism and Magnetic Materials **68**, 15 (1987).

¹⁷ J. Chaboy, L. M. García, F. Bartolomé, A. Marcelli, G. Cibir, H. Maruyama, S. Pizzini, A. Rogalev, J. B. Goedkoop, and J. Goulon, Phys. Rev. B **57**, 8424 (1998).

¹⁸ F. Bartolome, J. M. Tonnerre, N. Jaouen, D. Raoux, J. Chaboy, L. M. Garcia, H. Maruyama, and R. Steinmann, Journal of Applied Physics **87**, 4762 (2000).

¹⁹ G. M. Kalvius, D. R. Noakes, and O. Hartmann, *Handbook on the Physics and Chemistry of Rare Earths* (North-Holland, Amsterdam, 2001), vol. 32, chap. 206, pp. 55–451.

²⁰ A. Yaouanc and P. D. de Réotier, *Muon Spin Rotation, Relaxation, and Resonance, Application to Condensed Matter* (Oxford, New York, 2011).

²¹ A. Yaouanc, J. Budnick, E. Albert, M. Hama, A. Weidinger, R. Fruchart, P. L'heritier, D. Fruchart, and P. Wolfers, Journal of Magnetism and Magnetic Materials **67**, L286 (1987).

- ²² C. Niedermayer, A. Golnik, E. Recknagel, A. Weidinger, A. J. Yaouanc, P. L'Heritier, D. Fruchart, J. I. Budnick, and K. H. J. Buschow, *Hyperfine Interactions* **64**, 405 (1991).
- ²³ L. Ferreira, R. Guillen, P. Vulliet, A. Yaouanc, D. Fruchart, P. Wolfers, P. L'Heritier, and R. Fruchart, *Journal of Magnetism and Magnetic Materials* **53**, 145 (1985).
- ²⁴ Y. Takada, Y. Kaneko, K. Fukumoto, N. Miyamoto, A. Manabe, S. Imada, and S. Suga, *R&D Review of Toyota CRDL* **43**, 33 (2012).
- ²⁵ A. Suter and B. Wojek, *Physics Procedia* **30**, 69 (2012).
- ²⁶ P. Hohenberg and W. Kohn, *Phys. Rev.* **136**, B864 (1964).
- ²⁷ W. Kohn and L. J. Sham, *Phys. Rev.* **140**, A1133 (1965).
- ²⁸ D. Vanderbilt, *Phys. Rev. B* **41**, 7892 (1990).
- ²⁹ K. Miwa, *Phys. Rev. B* **84**, 094304 (2011).
- ³⁰ A. I. Liechtenstein, V. I. Anisimov, and J. Zaanen, *Phys. Rev. B* **52**, R5467 (1995).
- ³¹ K. Miwa, *Phys. Rev. B* **97**, 075143 (2018).
- ³² P. E. Blöchl, *Phys. Rev. B* **50**, 17953 (1994).
- ³³ K. Miwa and A. Fukumoto, *Phys. Rev. B* **65**, 155114 (2002).
- ³⁴ K. Miwa, N. Ohba, S.-i. Towata, Y. Nakamori, and S.-i. Orimo, *Phys. Rev. B* **69**, 245120 (2004).
- ³⁵ K. Miwa, *Phys. Rev. B* **84**, 094304 (2011).
- ³⁶ J. Sugiyama, K. Mukai, H. Nozaki, M. Harada, M. Månsson, K. Kamazawa, D. Andreica, A. Amato, and A. D. Hillier, *Phys. Rev. B* **87**, 024409 (2013).
- ³⁷ K. Miwa, *Phys. Rev. B* **97**, 075143 (2018).
- ³⁸ J. P. Perdew, K. Burke, and M. Ernzerhof, *Phys. Rev. Lett.* **77**, 3865 (1996).
- ³⁹ A. Alam, M. Khan, R. W. McCallum, and D. D. Johnson, *Applied Physics Letters* **102**, 042402 (2013).
- ⁴⁰ H.-S. Li, R. Mohanty, A. Raman, and C. Grenier, *Journal of Magnetism and Magnetic Materials* **162**, 301 (1996).
- ⁴¹ S. Barth, E. Albert, G. Heiduk, A. Möslang, A. Weidinger, E. Recknagel, and K. H. J. Buschow, *Phys. Rev. B* **33**, 430 (1986).
- ⁴² A. Schenck and F. N. Gygax, *Handbook of Magnetic Materials* (Elsevier, Amsterdam, 1995), vol. 9, chap. 2.
- ⁴³ J. Sugiyama, H. Nozaki, M. Månsson, K. Prša, D. Andreica, A. Amato, M. Isobe, and Y. Ueda, *Phys. Rev. B* **85**, 214407 (2012).
- ⁴⁴ M. Rosenberg, P. Deppe, M. Wójcik, and H. Stadelmeier, *Journal of Applied Physics* **57**, 4124 (1985).
- ⁴⁵ K. M. Kojima, J. Yamanobe, H. Eisaki, S. Uchida, Y. Fudamoto, I. M. Gat, M. I. Larkin, A. Savici, Y. J. Uemura, P. P. Kyriakou, et al., *Phys. Rev. B* **70**, 094402 (2004).
- ⁴⁶ R. Fruchart, P. L'Heritier, P. D. de Reotier, D. Fruchart, P. Wolfers, J. M. D. Coey, L. P. Ferreira, R. Guillen, P. Vulliet, and A. Yaouanc, *Journal of Physics F: Metal Physics* **17**, 483 (1987).
- ⁴⁷ H. V. Noort, D. D. Mooij, and K. Buschow, *Journal of the Less Common Metals* **115**, 155 (1986).
- ⁴⁸ S. S. Jaswal, *Phys. Rev. B* **41**, 9697 (1990).
- ⁴⁹ K. Hummler and M. Fähnle, *Phys. Rev. B* **53**, 3290 (1996).
- ⁵⁰ H. Moriya, H. Tsuchiura, and A. Sakuma, *Journal of Applied Physics* **105**, 07A740 (2009).
- ⁵¹ J. Wang, L. Liang, L. Zhang, L. Sun, and S. Hirano, *Journal of Applied Physics* **116**, 163917 (2014).
- ⁵² B. I. Min, J.-S. Kang, J. H. Hong, J. I. Jeong, Y. P. Lee, S. D. Choi, W. Y. Lee, C. J. Yang, and C. G. Olson, *Phys. Rev. B* **48**, 6217 (1993).
- ⁵³ H. Hiroyoshi, H. Yamauchi, Y. Yamaguchi, H. Yamamoto, Y. Nakagawa, and M. Sagawa, *Solid State Communications* **54**, 41 (1985).
- ⁵⁴ W. B. Yelon and J. F. Herbst, *Journal of Applied Physics* **59**, 93 (1986).
- ⁵⁵ R. Davis, R. Day, and J. Dunlop, *Solid State Communications* **56**, 181 (1985).
- ⁵⁶ M. Yamada, Y. Yamaguchi, H. Kato, H. Yamamoto, Y. Nakagawa, S. Hirosawa, and M. Sagawa, *Solid State Communications* **56**, 663 (1985).
- ⁵⁷ J. F. Herbst, C. D. Fuerst, and W. B. Yelon, *Journal of Applied Physics* **73**, 5884 (1993).
- ⁵⁸ J. F. Herbst and W. B. Yelon, *Journal of Applied Physics* **57**, 2343 (1985).
- ⁵⁹ P. Wolfers, S. Miraglia, D. Fruchart, S. Hirosawa, M. Sagawa, J. Bartolome, and J. Pannetier, *Journal of the Less Common Metals* **162**, 237 (1990).